

Non-Born-Oppenheimer study of the muonic molecule ion $^4He\mu^+$

Hang Yang(杨航), Meng-Shan Wu(吴孟山), Yi Zhang(张屹), Ting-Yun Shi(史庭云), Kalman Varga, Jun-Yi Zhang(张俊义)

Citation: Chin. Phys. B . 2020, 29(4): 043102 . **doi:** 10.1088/1674-1056/ab7908
Journal homepage: http://cpb.iphy.ac.cn; http://iopscience.iop.org/cpb

What follows is a list of articles you may be interested in

Relativistic calculations of fine-structure energy levels of He-like Ar in dense plasmas

Xiang-Fu Li(李向富), Gang Jiang(蒋刚)

Chin. Phys. B . 2018, 27(7): 073101 . **doi:** 10.1088/1674-1056/27/7/073101

Atomic structure and transition properties of H-like Al in hot and dense plasmas

Xiang-Fu Li(李向富), Gang Jiang(蒋刚), Hong-Bin Wang(王宏斌), Qian Sun(孙乾)

Chin. Phys. B . 2017, 26(1): 013101 . **doi:** 10.1088/1674-1056/26/1/013101

Calculations of the dynamic dipole polarizabilities for the Li^+ ion

Yong-Hui Zhang(张永慧), Li-Yan Tang(唐丽艳), Xian-Zhou Zhang(张现周), Ting-Yun Shi(史庭云)

Chin. Phys. B . 2016, 25(10): 103101 . **doi:** 10.1088/1674-1056/25/10/103101

Tune-out wavelengths for the alkaline-metal atoms

Wei-Wei Yu(于伟威), Rong-Mei Yu(于荣梅), Yong-Jun Cheng(程勇军) and Ya-Jun Zhou(周雅君)

Chin. Phys. B . 2016, 25(2): 023101 . **doi:** 10.1088/1674-1056/25/2/023101

High-precision spectroscopy of hydrogen molecular ions

Zhong Zhen-Xiang, Tong Xin, Yan Zong-Chao, Shi Ting-Yun

Chin. Phys. B . 2015, 24(5): 053102 . **doi:** 10.1088/1674-1056/24/5/053102

Non-Born–Oppenheimer study of the muonic molecule ion ^{4}Heμ^+*

Hang Yang(杨航)[1,2], Meng-Shan Wu(吴孟山)[1,†], Yi Zhang(张屹)[1,2], Ting-Yun Shi(史庭云)[1], Kalman Varga[3], and Jun-Yi Zhang(张俊义)[1]

[1] *State Key Laboratory of Magnetic Resonance and Atomic and Molecular Physics, Wuhan Institute of Physics and Mathematics, Chinese Academy of Sciences, Wuhan* 430071, *China*

[2] *University of Chinese Academy of Sciences, Beijing* 100049, *China*

[3] *Department of Physics and Astronomy, Vanderbilt University, Nashville, Tennessee* 37235, *USA*

(Received 2 January 2020; revised manuscript received 5 February 2020; accepted manuscript online 24 February 2020)

Accurate non-Born–Oppenheimer variational calculations of all bound states of the positive muon molecular ion ^{4}Heμ^+ have been performed using explicitly correlated Gaussian functions in conjunction with the global vectors. All the energies obtained are accurate in the order of 10^{-6} Hartree (1 Hartree = 27.2114 eV). Compared with the binding energies obtained from calculations based on the Born–Oppenheimer potential with the mass-weighted adiabatic corrections (*Chem. Phys. Lett.* **110** 487 (1984)), the largest relative deviation is up to 15%. By analyzing the average interparticle distances and possibility distributions of interparticle distances of this system, it is confirmed that the Born–Oppenheimer approximation is reasonable for this system and that ^{4}Heμ^+ can be regarded as a system of positive muon bound to a slightly distorted helium atom.

Keywords: positive muon, variational calculation, explicitly correlated Gaussian

PACS: 31.15.ac, 31.15.vn, 31.15.xt **DOI:** 10.1088/1674-1056/ab7908

1. Introduction

Positive muon μ^+, the antiparticle of muon, has attracted considerable attention and has been extensively studied. As a lepton, it plays an important role for testing the theory of quantum electrodynamics.[1–5] Moreover, it has also been used in searches for new physics beyond the Standard Model[6–10] As required by these applications, μ^+ should be trapped and cooled down to low temperature (around 10 eV) since the typical μ^+ beams have relatively high energies and poor phase space qualities.[11] Some high-precision and high-sensitivity μ^+ experiments are in progress, such as the muonium (Mu) spectroscopy experiment using microwave project (MuSEUM) at Japan Proton Accelerator Research Complex (JPARC)[5] and the Mu-MASS project at Paul Scherrer Institute (PSI).[12,13] Among these experiments, the helium buff gas is usually used in the precooling process due to its efficiency.

^{4}Heμ^+ was first observed by Fleming *et al.* in the thermalization process of μ^+ in the low-pressure He gas in 1981.[14] Interestingly, no muonium atom (μ^+e) was observed in the same thermalization process. Later, using the model of charge exchange collisions, Senba[15] well explained the experimental observation of Fleming *et al*. In addition, the slowing-down process of μ^+ in gas mixtures He–Ar and He–H_2, the process during which μ^+ is slowed from its initial MeV kinetic energy down to $\sim$ 10 eV by collisions with gas atoms, was also studied by Senba.[16]

The calculation[17] of ^{4}Heμ^+ was performed by Fournier and Lassier-Govers in 1982 using the Born–Oppenheimer (BO) potential for HeH^+ reported by Kolos and Peek[18] and combining with the appropriately mass-weighted adiabatic corrections calculated by Bishop and Cheung.[19] In 1984, Fournier and Le Roy improved their calculations for all bound levels of ^{4}Heμ^+ using a new interpolation procedure for the BO potential.[20] Because the positive muon is much like proton chemically (with the same charge and about 1/9 of proton's mass), it is acceptable to use the BO potential for HeH^+ in the calculations for ^{4}Heμ^+. The BO potential for HeH^+ was further improved by Cencek *et al.*[21] who expanded the wavefunctions at an internuclear distance of $R = 1.46$ a.u. (atomic unit) in terms of 600 explicitly correlated Gaussian (ECG) functions in 1995. Recently, using an expansion of 20000 generalized Heitler–London basis functions, Pachucki[22] obtained a very accurate BO potential with the precision of about 2×10^{-7} cm^{-1}. Later, new accurate potential curves for ^{4}HeH^+, ^{4}HeD^+, ^{3}HeH^+, ^{3}HeD^+ were generated by Tung *et al.*[23] using an expansion of 600 shifted centers ECG functions and including the adiabatic corrections. The accurate non-Born–Oppenheimer (non-BO) variational energies for bound states of ^{4}HeH^+ with zero orbital

*Project supported by the National Natural Science Foundation of China (Grant No. 11704399), the Strategic Priority Research Program of the Chinese Academy of Sciences (Grant No. XDB21030300), and the National Key Research and Development Program of China (Grant No. 2017YFA0304402).

†Corresponding author. E-mail: mswu@wipm.ac.cn

© 2020 Chinese Physical Society and IOP Publishing Ltd

angular momentum have been reported by Stanke *et al.*[24,25] However, for ^{4}Heμ^+, there is no *ab initio* calculation until now.

In this work, high-accuracy wavefunctions and energies for ^{4}Heμ^+ have been obtained by *ab-initio* calculations using ECG basis functions. To avoid the complicated one-by-one coupling of the orbital angular momenta, the global vector representation[26] is used. Convergence tests for the ground state energy and virial factor are given for examining the reliability of our calculations. The probability distributions and average values of interparticle distances are calculated in order to analyze the structure of ^{4}Heμ^+.

2. Theory

The total non-relativistic Hamiltonian for ^{4}Heμ^+ in the laboratory coordinate has the following form

$$\hat{H}_{\rm tot} = \sum_{i=1}^{4} \frac{\boldsymbol{p}_i^2}{2m_i} + \sum_{\substack{i,j=1 \\ j>i}}^{4} \frac{q_i q_j}{|\boldsymbol{r}_i - \boldsymbol{r}_j|}, \tag{1}$$

where $\boldsymbol{r}_i$, m_i, and q_i represent the position vector, the mass, and the charge of the i-th particle, respectively. Particle 1 and 2 refer to the He nucleus (α) and μ^+ while the last two stand for electrons.

To describe the intrinsic excitations of this system, the center-of-mass motion is subtracted from the total Hamiltonian, and the internal Hamiltonian has the following form

$$\hat{H} = \frac{1}{2}\sum_{i}^{3}\sum_{j}^{3}\Lambda_{ij}\boldsymbol{\pi}_i\cdot\boldsymbol{\pi}_j + \sum_{i=1}^{3}\frac{q_1 q_{i+1}}{|\boldsymbol{x}_i|} + \sum_{\substack{i,j=1 \\ j>i}}^{3}\frac{q_{i+1}q_{j+1}}{|\boldsymbol{x}_i - \boldsymbol{x}_j|}, \tag{2}$$

where

$$\Lambda_{ij} = \sum_{k=1}^{4} U_{ik}U_{jk}\frac{1}{m_k}, \quad (i,j=1,2,3),$$

$\boldsymbol{x}_i = \boldsymbol{r}_{i+1} - \boldsymbol{r}_1$ is the relative coordinate, and

$$\boldsymbol{\pi}_i = -\mathrm{i}\hbar\frac{\partial}{\partial \boldsymbol{x}_i}$$

is the momentum conjugate to $\boldsymbol{x}_i$. U refers to the transformation matrix defined by

$$\boldsymbol{x}_i = \sum_{j=1}^{4} U_{ij}\boldsymbol{r}_j, \quad \boldsymbol{r}_i = \sum_{j=1}^{4}(U^{-1})_{ij}\boldsymbol{x}_j, \quad (i=1,2,3,4), \tag{3}$$

where $\boldsymbol{x}_4$ is the center-of-mass coordinate.

The total wavefunction is expanded as

$$\Phi = \sum_{k=1}^{N} c_k(\phi_k + P_{34}\phi_k), \tag{4}$$

where P_{34} means the permutation of two electrons and ϕ_k is the ECG basis function. ECG basis functions were first introduced to quantum-chemical calculations by Boys and Singer in 1960.[27,28] Their matrix elements are analytically calculable and can be easily generalized for any N-body systems. Moreover, they are easily adaptable to the permutational symmetry of the interesting systems. Due to these major advantages, they are now widely used in the calculations of various few-body problems. In the present work, ϕ_k has the form

$$\phi_k = |\boldsymbol{v}|^{2K+L}\exp\Big[-\frac{1}{2}\boldsymbol{x}^{\rm T}A_k\boldsymbol{x}\Big]\,{\rm Y}_{LM}(\hat{\boldsymbol{v}})\chi, \tag{5}$$

where $\boldsymbol{x}^{\rm T} = (\boldsymbol{x}_1, \boldsymbol{x}_2, \boldsymbol{x}_3)$ and A_k is the k-th parameter matrix, $\boldsymbol{v} = \boldsymbol{u}^{\rm T}\boldsymbol{x}$ with $\boldsymbol{u}^{\rm T} = (u_1, u_2, u_3)$ is the global vector. ${\rm Y}_{LM}(\hat{\boldsymbol{v}})$ is the spherical harmonics while χ is the spin function. The global vector representation[26] simplifies the calculation of matrix elements by avoiding the complicated one-by-one coupling of the orbital angular momenta. Compared with the spherical ECG basis, the factor $|\boldsymbol{v}|^{2K+L}$ plays an important role in describing the increasing number of nodes for excited rovibrational states.

The energy and wavefunction for each state are obtained by minimizing the eigenvalue E through optimizing A_k, and by solving the general eigenvalue equation

$$Hc = EOc. \tag{6}$$

The optimization was carried out by the stochastic variational method (SVM) which has been proved to be efficient and accurate by various applications,[26–31] such as the calculation of the scattering length for the scattering between two ground state positronium atoms.[32] For simplicity, the values of $\boldsymbol{u}$ are set manually instead of being optimized automatically.

In the present study, the mass used for α and μ^+ are $m_\alpha = 7294.29954142\ m_{\rm e}$ and $m_{\mu^+} = 206.7682830\ m_{\rm e}$, which are the CODATA 2018 recommended values. Atomic units (a.u.) are used throughout the paper unless stated otherwise.

3. Calculations, results, and discussion

3.1. Convergence test

The convergence of the ground state energy for ^{4}Heμ^+ as a function of the basis-set size is shown in Table 1. As the reference for the binding energies of ^{4}Heμ^+, the ground state energy of ^{4}He obtained is -2.9033045577 a.u. by using 700 spherical ECG functions. In order to accurately describe the rovibration and orbital angular momentum coupling of ^{4}Heμ^+, three sets of $\boldsymbol{u}^{\rm T}$ are used, *i.e.*, $\boldsymbol{u}^{\rm T} = (1,0,0)$, $(0.5,0.5,0)$, and $(0.33,0.33,0.33)$. The energy obtained becomes lower as the basis-set size increases. Using 2800 ECGs,

we get the ground state energy accurate in the order of 10^{-8} Hartree. Usually, the convergences of the wavefunctions are slower than those of energies. In order to check the quality of the ground state wavefunction, the virial factor η is also calculated and shown in Table 1. The virial factor is defined as

$$\eta = \left| 1 + \frac{\langle V \rangle}{2\langle T \rangle} \right|, \tag{7}$$

where $\langle T \rangle$ and $\langle V \rangle$ are the expectation values of the kinetic energy operator and potential energy operator, respectively. The closer to zero that η is, the better quality the ground state wavefunction has. From Table 1 we can see that both $\langle T \rangle$ and $\langle V \rangle$ have eight significant digits and the smallest η is in the order of 10^{-9}.

Table 1. The convergences of the total energy, the expectation values of kinetic energy operator and potential energy operator, and the virial factor for the ground state ^{4}Heμ^+.

Basis size	Energy	$\langle T \rangle$	$\langle V \rangle$	η
2000	−2.95914547	2.95914558	−5.91829105	1.77×10^{-8}
2400	−2.95914548	2.95914553	−5.91829102	8.23×10^{-9}
2800	−2.95914549	2.95914555	−5.91829105	9.55×10^{-9}

3.2. Expectation values of energies

For each of the rovibrational excited states, the largest basis-set size and the global vectors used are the same as the corresponding for the ground state. Compared with the ground state, larger values of K in Eq. (5) are used for higher rovibrational states. For the v-th vibrational state, $0 \le K \le v$ is used. Consequently, it is more difficult and time-consuming for the calculations of high excited states. Due to the slower convergences, seven significant digits are obtained for the energies of some high excited states. Comparison of our results for binding energies ($E^{\rm b}$) and those of Fournier and Le Roy[20] ($E^{\rm b}_{\rm FL}$) is shown in Table 2. The parameter $\Delta = |(E^{\rm b} - E^{\rm b}_{\rm FL})/E^{\rm b}|$ represents the relative deviation. The rovibrational bound levels are denoted as (j, v) with j and v being the rotational and vibrational quantum numbers, respectively. All our non-BO values for the binding energies are larger than the previous BO results of Fournier and Le Roy as the relative deviations increase along with the increase of j and v. The most weakly bound state is the $(j = 4, v = 2)$ state with the binding energy 14.576 cm^{-1} for which the two approaches have the largest relative deviation, *i.e.*, about 15%.

Table 2. Comparisons of the binding energies we obtained ($E^{\rm b}$, in units of cm^{-1}) with those of Fournier and Le Roy[20] ($E^{\rm b}_{\rm FL}$) for ^{4}Heμ^+. The parameter $\Delta = |(E^{\rm b} - E^{\rm b}_{\rm FL})/E^{\rm b}|$ represents the relative deviation.

j	$v=0$	$E^{\rm b}_{\rm FL}$ [20]	Δ	$v=1$	$E^{\rm b}_{\rm FL}$ [20]	Δ	$v=2$	$E^{\rm b}_{\rm FL}$ [20]	Δ	$v=3$	$E^{\rm b}_{\rm FL}$ [20]	Δ
0	12255.670	12255.5	1.38×10^{-5}	5849.424	5849.0	7.25×10^{-5}	1768.258	1766.7	8.81×10^{-4}	134.752	134.2	4.10×10^{-3}
1	11805.442	11804.9	4.59×10^{-5}	5509.037	5508.4	1.16×10^{-4}	1553.094	1551.4	1.09×10^{-3}	69.972	69.6	5.31×10^{-3}
2	10924.802	10923.6	1.10×10^{-4}	4848.101	4847.1	2.07×10^{-4}	1146.993	1145.0	1.74×10^{-3}			
3	9652.028	9650.0	2.10×10^{-4}	3905.776	3904.3	3.78×10^{-4}	601.933	599.6	3.88×10^{-3}			
4	8041.521	8038.7	3.51×10^{-4}	2740.099	2738.2	6.93×10^{-4}	14.576	12.4	1.49×10^{-1}			
5	6161.176	6157.6	5.80×10^{-4}	1430.195	1427.9	1.61×10^{-3}						
6	4090.486	4086.5	9.74×10^{-4}	89.827	87.2	2.93×10^{-2}						
7	1921.391	1917.3	2.13×10^{-3}									

3.3. Expectation values of interparticle distances

The expectation values of interparticle distances and the virial factors for all the bound states of ^{4}Heμ^+ are shown in Table 3. In order to provide a direct-viewing feeling, the expectation values of interparticle distances are illustrated in Fig. 1. For simplicity, we number all bound states in sequence. From Fig. 1(a) we can see that the average distances between α and μ^+ ($\langle r_{\alpha-\mu^+} \rangle$) increase quickly with the vibrational excitations and slowly with the rotational excitations. The $(j = 1, v = 3)$ state has the longest distance for $\langle r_{\alpha-\mu^+} \rangle$. It can be seen from Fig. 1(b) that the distances between μ^+ and the electron ($\langle r_{\mu^+-{\rm e}} \rangle$) have the same trend as $\langle r_{\alpha-\mu^+} \rangle$. Moreover, the values of $\langle r_{\mu^+-{\rm e}} \rangle$ are very close to those of $\langle r_{\alpha-\mu^+} \rangle$, *i.e.*, $\langle r_{\mu^+-{\rm e}} \rangle \approx \langle r_{\alpha-\mu^+} \rangle$ as shown in Table 3. Figure 1(c) shows that the distances between α and the electron ($\langle r_{\alpha-{\rm e}} \rangle$) first slightly increase and then decrease as v increase for $0 \le j \le 4$. Generally, $\langle r_{\alpha-{\rm e}} \rangle$ changes slightly around 0.95 a.u. The distances between two electrons ($\langle r_{{\rm e}-{\rm e}} \rangle$) show the same trend as $\langle r_{\alpha-{\rm e}} \rangle$, see Fig. 1(d). To make a comparison, $\langle r_{\alpha-{\rm e}} \rangle = 0.9296$ a.u. and $\langle r_{{\rm e}-{\rm e}} \rangle = 1.4222$ a.u. are also calculated for the ground state of ^{4}He atom. Consequently, the deviations for $\langle r_{\alpha-{\rm e}} \rangle$ and $\langle r_{{\rm e}-{\rm e}} \rangle$ between ^{4}He and ^{4}Heμ^+ are small, *i.e.*, $\langle r_{\alpha-{\rm e}} \rangle_{{\rm He}\mu^+} \approx \langle r_{\alpha-{\rm e}} \rangle_{\rm He}$ and $\langle r_{{\rm e}-{\rm e}} \rangle_{{\rm He}\mu^+} \approx \langle r_{{\rm e}-{\rm e}} \rangle_{\rm He}$. Therefore, it is reasonable to conclude that ^{4}Heμ^+ can be treated as a μ^+ particle weakly bound to a slightly distorted ^{4}He.

Table 3. The average interparticle distances (in units of a.u.) and the virial factors for all bound states of ^{4}Heμ^+.

No.	(j,v)	$\langle r_{\alpha-\mu^+}\rangle$	$\langle r_{\alpha-e}\rangle$	$\langle r_{\mu^+-e}\rangle$	$\langle r_{e-e}\rangle$	$\langle r^2_{\alpha-\mu^+}\rangle$	$\langle r^2_{\alpha-e}\rangle$	$\langle r^2_{\mu^+-e}\rangle$	$\langle r^2_{e-e}\rangle$	η
1	(0,0)	1.6221	0.9416	1.6616	1.4184	2.7091	1.2043	3.1581	2.4654	9.55×10^{-9}
2	(0,1)	2.0236	0.9547	2.0531	1.4495	4.3648	1.2623	4.8340	2.6050	5.12×10^{-9}
3	(0,2)	2.7387	0.9529	2.7730	1.4545	8.1219	1.2714	8.7005	2.6465	1.54×10^{-7}
4	(0,3)	5.0912	0.9354	5.1370	1.4308	28.3601	1.2151	29.2245	2.5545	2.05×10^{-7}
5	(1,0)	1.6343	0.9427	1.6727	1.4205	2.7499	1.2078	3.1984	2.4734	3.47×10^{-9}
6	(1,1)	2.0439	0.9553	2.0729	1.4508	4.4526	1.2646	4.9235	2.6107	1.96×10^{-8}
7	(1,2)	2.7916	0.9525	2.8263	1.4543	8.4378	1.2707	9.0251	2.6462	2.50×10^{-7}
8	(1,3)	5.6295	0.9341	5.6744	1.4289	35.0737	1.2103	35.9701	2.5462	2.55×10^{-7}
9	(2,0)	1.6589	0.9449	1.6954	1.4247	2.8334	1.2148	3.2810	2.4891	1.41×10^{-9}
10	(2,1)	2.0860	0.9564	2.1142	1.4533	4.6382	1.2691	5.1130	2.6215	3.99×10^{-8}
11	(2,2)	2.9115	0.9516	2.9472	1.4535	9.1787	1.2684	9.7858	2.6440	2.97×10^{-7}
12	(3,0)	1.6967	0.9480	1.7304	1.4308	2.9644	1.2251	3.4108	2.5122	4.36×10^{-10}
13	(3,1)	2.1539	0.9579	2.1811	1.4568	4.9463	1.2751	5.4280	2.6366	2.66×10^{-8}
14	(3,2)	3.1459	0.9496	3.1836	1.4512	10.7296	1.2625	11.3743	2.6361	9.01×10^{-9}
15	(4,0)	1.7491	0.9518	1.7794	1.4385	3.1513	1.2383	3.5968	2.5422	7.10×10^{-9}
16	(4,1)	2.2562	0.9592	2.2826	1.4605	5.4307	1.2817	5.9246	2.6540	5.58×10^{-8}
17	(4,2)	3.7775	0.9443	3.8191	1.4442	15.7829	1.2458	16.5121	2.6094	2.11×10^{-7}
18	(5,0)	1.8187	0.9563	1.8452	1.4476	3.4090	1.2541	3.8544	2.5782	1.06×10^{-8}
19	(5,1)	2.4141	0.9599	2.4405	1.4636	6.2274	1.2872	6.7434	2.6704	1.48×10^{-8}
20	(6,0)	1.9106	0.9609	1.9331	1.4575	3.7662	1.2716	4.2136	2.6189	3.54×10^{-9}
21	(6,1)	2.7078	0.9584	2.7366	1.4637	7.8913	1.2865	8.4541	2.6770	4.99×10^{-8}
22	(7,0)	2.0359	0.9653	2.0550	1.4675	4.2865	1.2898	4.7405	2.6624	1.00×10^{-8}

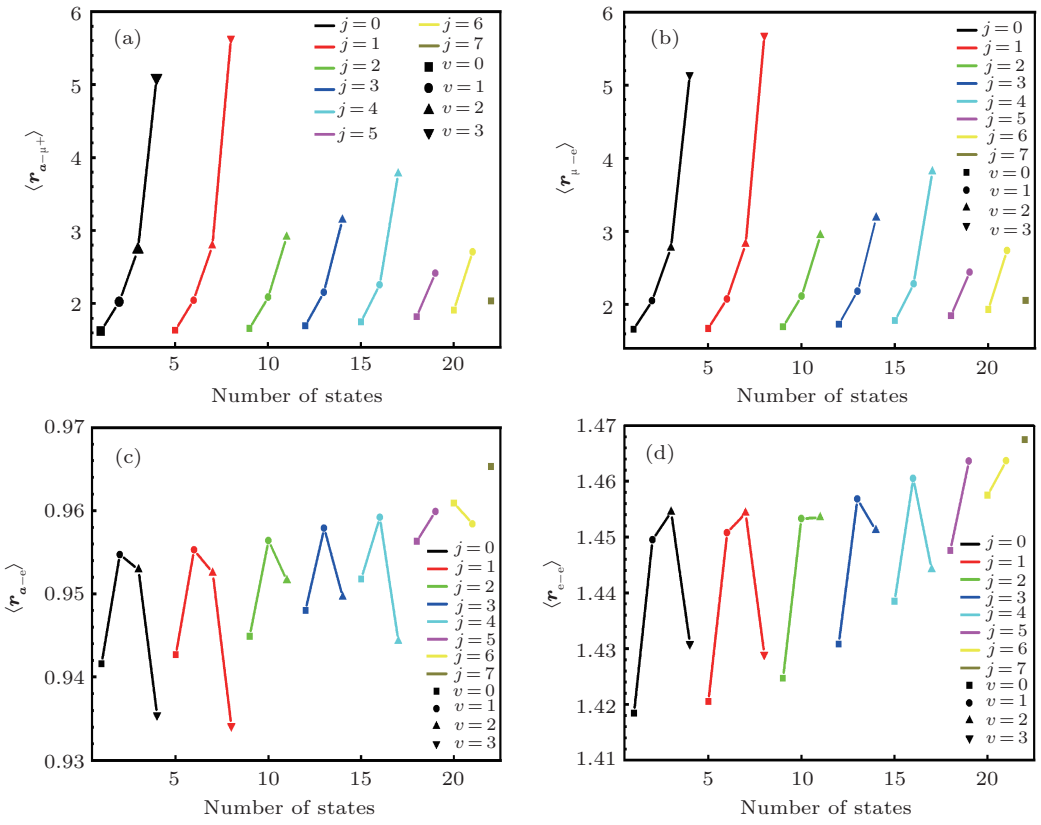


Fig. 1. The average interparticle distances (in units of a.u.) for all bound states of ^{4}Heμ^+.

Furthermore, the comparison of average interparticle distances between ^{4}Heμ^+ and ^{4}He H$^+$ is shown in Table 4. Due to the lighter mass of μ^+, for the case of the zero total angular momentum, ^{4}Heμ^+ has only four bound states. However, there exist twelve bound states of ^{4}He H$^+$ for the same case. Though the average interparticle distances of the ground state ^{4}Heμ^+ are close to those of ^{4}He H$^+$ the average interparticle distances for ^{4}Heμ^+ are much larger for the excited states. In other words, ^{4}He H$^+$ are more tightly bounded than ^{4}Heμ^+.

Table 4. Comparison of the average interparticle distances (in units of a.u.) between ^{4}He μ^+ and ^{4}He H^+.[33]

	^{4}He μ^+				^{4}He H^+			
(j,ν)	$\langle r_{\alpha-\mu^+}\rangle$	$\langle r_{\alpha-e}\rangle$	$\langle r_{\mu^+-e}\rangle$	$\langle r_{e-e}\rangle$	$\langle r_{\alpha-H^+}\rangle$	$\langle r_{\alpha-e}\rangle$	$\langle r_{H^+-e}\rangle$	$\langle r_{e-e}\rangle$
(0,0)	1.6221	0.9416	1.6616	1.4184	1.5177	0.9356	1.5619	1.4052
(0,1)	2.0236	0.9547	2.0531	1.4495	1.6339	0.9430	1.6718	1.4210
(0,2)	2.7387	0.9529	2.7730	1.4545	1.7650	0.9491	1.7981	1.4346
(0,3)	5.0912	0.9354	5.1370	1.4308	1.9164	0.9535	1.9463	1.4455

3.4. Probability density distribution of interparticle distances

Compared with the average interparticle distances, the probability density distribution of interparticle distances will give more information about the structure of ^{4}Heμ^+. The probability density of distance between particle i and j is given by

$$\rho(r_{i-j}) = \int \mathrm{d}\Omega_{\boldsymbol{r}_{i-j}} \left\langle \Phi \middle| \delta\Big(\sum_{k=1}^{3} c_k \boldsymbol{x}_k - \boldsymbol{r}_{i-j}\Big) \middle| \Phi \right\rangle r_{i-j}^2 , \tag{8}$$

where Φ is the wavefunction of a bound state, $\boldsymbol{r}_{i-j} = \boldsymbol{r}_i - \boldsymbol{r}_j$, $\langle \cdots \rangle$ means the integration of relative coordinates $(\boldsymbol{x_1}, \boldsymbol{x_2}, \boldsymbol{x_3})$ and $\int \mathrm{d}\Omega_{\boldsymbol{r}_{i-j}}$ means the integration over the angle of $\boldsymbol{r}_{i-j}$. $\rho(r_{i-j})$ can be obtained easily since the matrix elements for Dirac delta function δ can be analytically calculated.

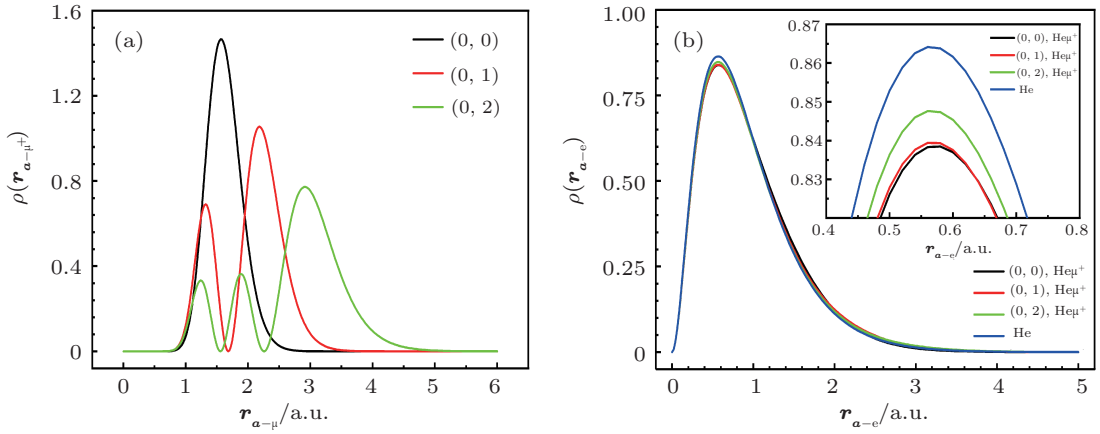


Fig. 2. Probability density distributions of $\rho(r_{\alpha-\mu^+})$ and $\rho(r_{\alpha-e})$ for the $(j=0,\nu=0,1,2)$ states. In panel (b), $\rho(r_{\alpha-e})$ for ^{4}He is also shown.

Figures 2(a) and 2(b) plot the probability densities $\rho(r_{\alpha-\mu^+})$ and $\rho(r_{\alpha-e})$ for $(j=0,\nu=0,1,2)$ as functions of $r_{\alpha-\mu^+}$ and $r_{\alpha-e}$, respectively. $\rho(r_{\alpha-\mu^+})$ of excited bound states have the larger spatial extension than that of the ground state while the number of nodes for $\rho(r_{\alpha-\mu^+})$ is equal to the vibrational quantum number ν. As shown in Fig. 2(b), the electrons are centered around α and their probability distributions are almost the same for different states. In addition, $\rho(r_{\alpha-e})$ of ^{4}He is also shown in Fig. 2(b) to make a comparison. Generally, $\rho(r_{\alpha-e})$ of ^{4}He μ^+ is only little different from $\rho(r_{\alpha-e})$ of ^{4}He. Interestingly, for He μ^+ with $j=0$ and $0\le\nu\le 2$, $\rho(r_{\alpha-e})$ becomes larger along with the increase of ν for $r_{\alpha-e} < 1$ a.u. while they are all smaller than $\rho(r_{\alpha-e})$ of He in the same region of $r_{\alpha-e}$. This can be explained with two reasons: Firstly, the electrons are attracted by μ^+ and hence slightly deviate from α. Secondly, the attraction of μ^+ becomes weaker for higher excited states as the distances between μ^+ and electrons are larger.

4. Summary

For the first time, non-BO calculations are carried out for the structural properties of ^{4}He μ^+ using ECGs with the global vector representation together. Overall, the non-BO energies for the rovibrational bound states are accurate in the order of 10^{-6} Hartree. Compared with the BO values of binding energies obtained by Fournier and Le Roy, all the corresponding non-BO values are larger. The largest relative deviation between them is about 15% for the most weakly bound state with $j=4$ and $\nu=2$. In addition, the expectations and probability density distributions of interparticle distances are discussed in detail to confirm that ^{4}Heμ^+ can be regarded as a system of μ^+ bound to a slightly distorted ^{4}He and hence that the BO approximation is reasonable for this system.

References

[1] Rich A 1981 *Rev. Mod. Phys.* **53** 127
[2] Karshenboim S G 2005 *Phys. Rep.* **422** 1

[3] Jungmann K P 2006 *Nucl. Phys. B-Proc. Suppl.* **155** 355
[4] Khaw K S, Antognini A, Prokscha T, Kirch K, Liszkay L, Salman Z and Crivelli P 2016 *Phys. Rev. A* **94** 022716
[5] Crivelli P 2018 *Hyperfine Interact.* **239** 49
[6] Willmann L, Schmidt P V, Wirtz H P, *et al.* 1999 *Phys. Rev. Lett.* **82** 49
[7] Bennett G W, Bousquet B, Brown H N, *et al.* 2004 *Phys. Rev. Lett.* **92** 161802
[8] Karshenboim S G 2010 *Phys. Rev. Lett.* **104** 220406
[9] Karshenboim S G, McKeen D, and Pospelov M 2014 *Phys. Rev. D* **90** 073004
[10] Frugiuele C, Pérez-Ríos J and Peset C 2019 *Phys. Rev. D* **100** 015010
[11] Taqqu D 2006 *Phys. Rev. Lett.* **97** 194801
[12] Bao Y, Antognini A, Bertl W, *et al.* 2014 *Phys. Rev. Lett.* **112** 224801
[13] Belosevic I, Antognini A, Bao Y, *et al.* 2019 *Hyperfine Interact.* **240** 41
[14] Fleming D G, Mikula R J and Garner D M 1981 *Hyperfine Interact.* **8** 307
[15] Senba M 1988 *J. Phys. B: At. Mol. Opt. Phys.* **21** 3093
[16] Senba M, Arseneau D J, Pan J J and Fleming D G 2006 *Phys. Rev. A* **74** 042708
[17] Fournier P G and Lassier-Govers B 1982 *J. Physique Lett.* **43** 483
[18] Kołos W and Peek J 1976 *Chem. Phys.* **12** 381
[19] Bishop D M and Cheung L M 1979 *J. Mol. Spectrosc.* **75** 462
[20] Fournier P G and Roy R J L 1984 *Chem. Phys. Lett.* **110** 487
[21] Cencek W, Komasa J and Rychlewski J 1995 *Chem. Phys. Lett.* **246** 417
[22] Pachucki K 2012 *Phys. Rev. A* **85** 042511
[23] Tung W C, Pavanello M and Adamowicz L 2012 *J. Chem. Phys.* **137** 164305
[24] Stanke M, Kedziera D, Molski M, Bubin S, Barysz M and Adamowicz L 2006 *Phys. Rev. Lett.* **96** 233002
[25] Stanke M, Kedziera D, Bubin S and Adamowicz L 2008 *Phys. Rev. A* **77** 022506
[26] Varga K and Suzuki Y 1995 *Phys. Rev. C* **52** 2885
[27] Mitroy J, Bubin S, Horiuchi W, *et al.* 2013 *Rev. Mod. Phys.* **85** 693
[28] Bubin S, Pavanello M, Tung W C, Sharkey K L and Adamowicz L 2013 *Chem. Rev.* **113** 36
[29] Varga K and Suzuki Y 1996 *Phys. Rev. A* **53** 1907
[30] Usukura J, Suzuki Y and Varga K 1999 *Phys. Rev. B* **59** 5652
[31] Mitroy J, Zhang J Y and Varga K 2008 *Phys. Rev. Lett.* **101** 123201
[32] Ivanov I A, Mitroy J and Varga K 2001 *Phys. Rev. Lett.* **87** 063201
[33] Bubin S 2006 *Accurate Non-Born–Oppenheimer Variational Calculations Of Small Molecular Systems* (PhD Dissertation) (Tucson: The University of Arizona)